GeoVirtual 2020 September 14-16 Resilience and Innovation

Constitutive modeling uniaxial compressive behaviors of an artificial frozen sandy clay at different temperatures

Sohail Akhtar & Biao Li
Department of Building, Civil & Environmental Engineering, Concordia University, Montreal, Quebec, Canada, H3G 1M8

ABSTRACT
Frozen soil has a rheological behavior close to the soft rock category and the rate-dependent behavior of frozen clay soil is complicated. A large number of experimental studies illustrated the rate-dependent mechanical behaviors of frozen soil which was reflected by creep deformations, stress relaxations, and rate-dependent stress-strain relations. Nevertheless, there were limited studies on constitutive modeling of the time-dependent stress-strain behavior of frozen clay soils at different frozen temperatures. The objective of this study is to numerically investigate the time-dependent behavior of an artificial frozen clay soil at temperature ranges from -2ºC to -15ºC. The Drucker-Prager model is adopted along with the Singh-Mitchell creep model to simulate time-dependent uniaxial compression behaviors of frozen sandy clay soil samples. The constitutive modeling is validated against a series of uniaxial compressive test results, where results show that a high deformation rate tends to generate brittle failure with post-peak softening behavior and a low deformation rate result in a diffuse failure associated with strain hardening.

RÉSUMÉ

Le sol gelé a un comportement rhéologique proche de la catégorie des roches molles et le comportement dépendant de la vitesse du sol argileux gelé est compliqué. Un grand nombre d'études expérimentales ont illustré les comportements mécaniques dépendants de la vitesse du sol gelé qui se reflétaient par des déformations de fluage, des relaxations de contrainte et des relations contrainte-déformation dépendant de la vitesse. Néanmoins, il y avait peu d'études sur la modélisation constitutive du comportement contrainte-déformation en fonction du temps des sols argileux gelés à différentes températures gelées. L'objectif de cette étude est d'étudier numériquement le comportement dépendant du temps d'un sol argileux gelé artificiel à des températures de -2ºC à -15 ºC. Le modèle Drucker-Prager est adopté avec le modèle de fluage Singh-Mitchell pour simuler les comportements de compression uniaxiale en fonction du temps de deux sols argilo-sableux gelés. La modélisation constitutive est validée par rapport à une série de résultats d'essais de compression uniaxiale, où les résultats montrent qu'un taux de déformation élevé a tendance à générer une rupture fragile avec un comportement de ramollissement post-pic et une faible vitesse de déformation entraîne une rupture diffuse associée à l'écrouissage.

1 INTRODUCTION

The long-term stability analysis of frozen soil (i.e. seasonal frozen, permafrost, and artificially frozen) attracted the attention of researchers to study the time-dependent strength degradation with the increase of construction activities involving frozen soil in foundations. Temperature and time-dependent mechanical properties play a key role in terms of stability and safety for every type of construction industry. The mechanical strength parameters and deformation behavior of frozen soil are highly dependent on strain rate, applied stress, mineralogy, and frozen temperature. As seasonally frozen soil typically occurs at shallow depths where a low confining pressure can be assumed, its stress-strain behavior is little affected by confining pressure. A series of studies were conducted to investigate the uniaxial compressive behavior of frozen soil due to its efficiency and effectiveness (Zhu and Carbee. 1984; Li et al. 2004; Zhao et al. 2009; Chen et al. 2011; Fei and Yang. 2019). The deformation behaviors (i.e. brittle or ductile) of frozen soil are mainly governed by the applied loading rate and temperature conditions (Arenson and Springman, 2005). The strong viscous behavior should be related to the available unfrozen water content in the frozen soil. As is shown in Fig. 1, the research work by Nixon (1991) gives a relationship between unfrozen water content and

temperature by a non-linear power law equation ($W_u = A(-T)^B$).

Previously, various researchers using creep models (Ladanyi. 1972; Hou et al. 2018) and stress relaxation models (Ladanyi and Benyamina 1995; Wang et al. 2011) to study the time-dependent rheological behavior of frozen soil. The developed models cannot simulate the time-dependent compressive behavior of frozen soil at different temperatures. In this study, a series of uniaxial compression test were performed on artificial frozen sandy clay soil samples at different temperatures. Finite element modeling was conducted using Drucker-Prager model incorporated with Singh-Mitchell creep model to investigate the temperature and strain-rate dependent stress-strain relations.

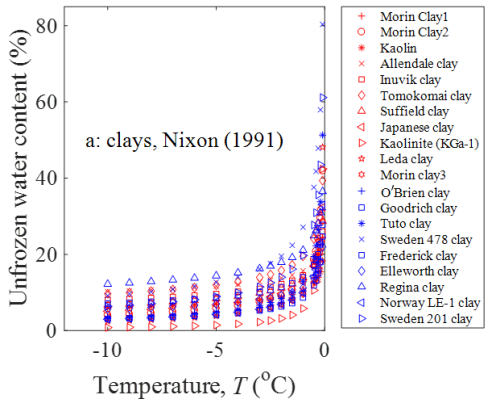

(a)

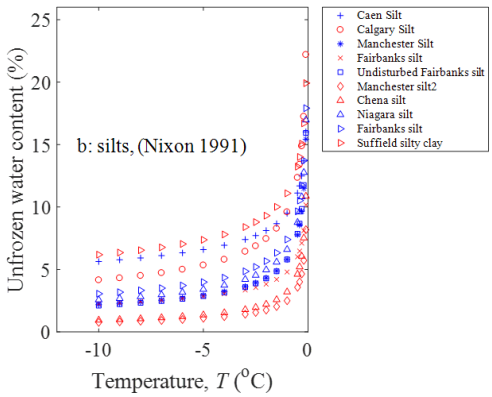

(b)

Figure 1 Graphs showing unfrozen water content of (a) clays and (b) silts at varying frozen temperatures, after Nixon (1991).

2 CONSTITUTIVE MODELS ADOPTED FOR FINITE ELEMENT SIMULATION

In this study, instantaneous elastic and plastic deformation is determined by the linear Drucker-Prager model and viscoplastic or time-dependent plastic deformation is determined by the Singh-Mitchell model using Abaqus (2016).

2.1 Drucker-Prager model

The Drucker-Prager model has been widely used in the numerical analysis of geotechnical problems (Helwany. 2007). The linear Drucker-Prager yield criterion is given by Eq. 1.

$$F = t - p\tan\beta - d \qquad [1]$$

where $t = \frac{1}{2}q\left[1+\frac{1}{K}-\left(1-\frac{1}{K}\right)\left(\frac{r}{q}\right)^3\right]$, in this study K=1, is assumed, therefore $t = q$; p is the mean effective stress which can be defined by the effective stress tensor σ as, $p = \frac{1}{3}trace(\sigma)$; q is the von Mises equivalent stress, which can be defined by the deviatoric stress tensor as, $q = \sqrt{\frac{3}{2}\mathbf{S}:\mathbf{S}}$, where $\mathbf{S}$ is the deviatoric stress tensor defined as, $\mathbf{S} = \boldsymbol{\sigma} - p\mathbf{I}$ and $\mathbf{I}$ is the identity matrix; d is the Drucker-Prager cohesion can be defined as, $d = \left(1-\frac{1}{3}\tan\beta\right)\sigma_c$, σ_c is the uniaxial compression yield stress; and β is the angle of friction in the p-q space.

2.2 Singh-Mitchell creep model

Based on this model, there is two separate and independent creep mechanism. One is shear creep which is controlled by cohesion mechanism ($d\varepsilon_s^{cr}$) and the second is consolidation creep which is attributed to consolidation mechanism ($d\varepsilon_c^{cr}$). The total creep strain is a combination of these two components:

$$d\varepsilon^{cr} = d\varepsilon_s^{cr} + d\varepsilon_c^{cr} \qquad [2]$$

As in this study, we only need to consider the shear creep and the consolidation creep is ignored ($d\varepsilon_c^{cr} = 0$). The creep potential function for cohesion mechanics can be written as,

$$g_s^{cr} = \sqrt{\left(0.1\frac{d}{(1-\frac{1}{3}\tan\beta)}\tan\beta\right)^2 + q^2} - p\tan\beta \qquad [3]$$

The Singh-Mitchell creep model for the shear creep takes the form as:

$$\dot{\varepsilon}_1 = A^s e^{\alpha^s \sigma_{cr}^s} \left(\frac{t_1}{t}\right)^{m^s} \quad [4]$$

where A^s, α^s, and m^s are three creep parameters that are back-calculated from the lab stress relaxation test performed on frozen sandy clay soil. And also, σ_{cr}^s is the equivalent creep stress, determined as the intersection of the equivalent creep surface with the uniaxial compression curve by the following expression,

$$\sigma_{cr}^s = \frac{q - p\tan\beta}{\left(1 - \frac{1}{3}\tan\beta\right)} \quad [5]$$

3 RESULTS OF UNIAXIAL COMPRESSIVE TESTS AND NUMERICAL ANALYSIS

3.1 Experimental results

A series of uniaxial compressive tests were conducted on artificially frozen soil samples composed of silica sand 7030 (50 % by weight) and Bentonite Western 325M (50% by weight) (Girgis, 2019). According to ASTM D4083-2016, the prepared soil is classified as high plastic inorganic sandy clay. Atterberg limits and other physical properties of this soil mixture is given in table 1.

Table 1. Atterberg limits data and other physical properties of the soil before freezing

Parameters	Bentonite-Sand
Bulk Density (g/cm3)	1.53
Water content[1] (%)	59
Specific gravity	2.63
Liquid limit (%)	97
Plastic limit (%)	34
Plastic Index (%)	63
Sand (%)	50
Clay (%)	50

[1]water content of specimens after preparation

A series of laboratory tests were carried out on those artificial frozen sandy clay soils to measure the rate-dependent uniaxial compressive behavior at temperatures ranging from -15°C to -2°C. Different post-failure modes were observed for samples as shown in Figure 2. Three different loading rates (i.e. 1mm/min, 3mm/min, and 9mm/min) were used to observe the time-dependent strength degradation at various frozen temperatures. At a lower temperature, less external disintegration is observed as compared to the case with a higher temperature. While this difference is insignificant at a higher loading rate. The degradation behavior of the physical-mechanical strength parameters of frozen sandy clayey soil during uniaxial compression loading depends on the frozen temperature and loading rate. The schematic view of deformation modes depending on loading rate and temperature conditions in the two unique phenomenal curves is shown in Figure 3, are summarized in the following:

1. At lower temperatures (-15ºC, -10ºC, and -5ºC) and higher loading rates, the frozen soil has three unique and distinctive modes of deformation (i.e. linear elastic, plastic hardening, and shear softening) as shown in Figure 3 (a).
2. At higher temperatures (-2ºC) and lower loading rates, the frozen soil yields only two modes of deformation (i.e. linear elastic and plastic hardening) as shown in Figure 3 (b).

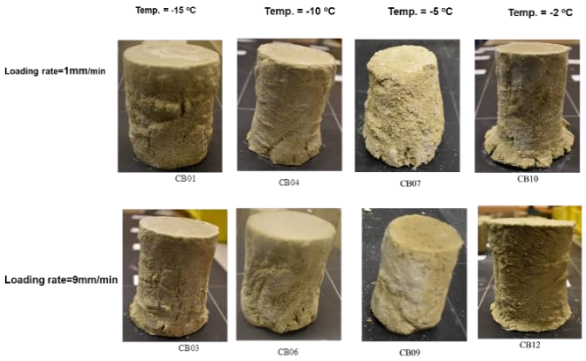

Figure 2. Post-failure photos of UCS test samples at different applied temperatures and deformation rates, (CB = bentonite-sand samples).

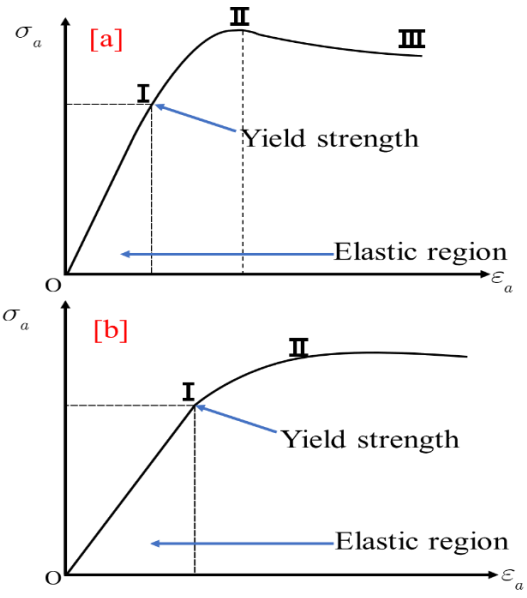

Figure 3. Schematic view of failure modes in the frozen sandy clayey soil under the uniaxial compression test.

Figure 4 shows the relationship between the yield strength (the upper bound of stress for linear elastic deformation) and the frozen temperature under three different loading conditions. It can be seen in Figure 4, with the increase of temperature, frozen soil shows lower yield strength, and a linear relation can be used to quantify this temperature-dependent behavior. With the decrease of temperature, unfrozen water fraction decreases, which leads to an increase in ice cementation and an increase of cohesion strength. Figure 4 also displays the effect of deformation rate on yield strengths. The difference in yield strengths is more significant at colder temperature condition (e.g., -15°C) than that of warmer temperature condition (-2°C). Such a difference should be closely related to the strong viscous behavior of unfrozen water presented in the pore space. It can be seen in Figure 4, the yield strength decreases by 6 times when the temperature increases from -15°C to -2°C, at a loading rate of 9mm/min. However, the yield strength yields 2 times less when loading rate decreases from 9mm/min to 1mm/min, at a constant temperature of -15°C.

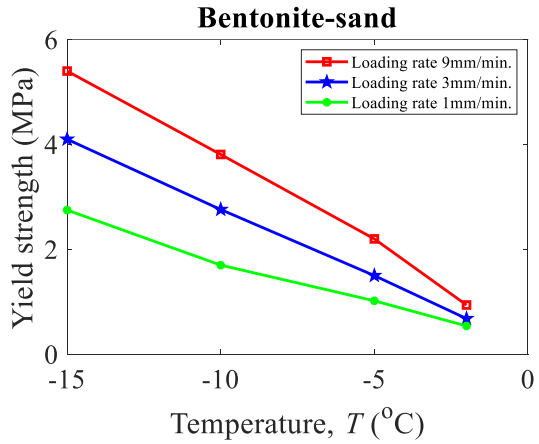

Figure 4. Measured relations of yield strengths and applied temperatures at different deformation rates.

3.2 Numerical model and input parameters

We used Abaqus to conduct finite element modeling of laboratory tests. Linear Drucker-Prager model is used along with Singh-Mitchell creep law to characterize the time-dependent deformation behavior. A displacement-controlled condition is applied on the top of the soil sample and the bottom is kept fixed while the temperatures of the frozen are held constant as an analogy to the condition in laboratory tests (Girgis, 2019). For the numerical analysis, required input parameters are given in Table 2 along with the references and methods through which these parameters are acquired. The dilation angle is determined according to Bolton (1986) and given by Eq. 6.

Table 2. Summary of some physical properties of Hong Kong marine deposit soil for numerical modeling.

Parameters	value	Reference
Peak friction angle, ϕ_{max} (degrees)	16.5	Li and Wong (2016)
Residual friction angle, ϕ_{cri} (degrees)	10	Li and Wong (2016)
Dilation angle, ψ (degrees)	7	Bolton (1986)
Drucker-Prager friction angle β (degrees)	15	Helwany (2007)

The finite element model along with the generated mesh and the location of monitoring points (i.e. Point 1 is for vertical stress and axial strain and Point 4 is for lateral strain) are illustrated in Figure 5. The size of the simulated sample is according to those used in laboratory tests (4.5 inches in height and 2 inches in diameter). The mesh is kept small enough that with further increase in mesh numbers does not affect the overall results. Thus, a mesh convergency was validated. It should be noted that the selected monitoring point for the lateral strain is of maximum intensity of strain.

$$0.8\psi = \varphi - \varphi_c \qquad [6]$$

Here ψ is the dilation angle; φ and φ_c are frictional angle and residual friction angle respectively.

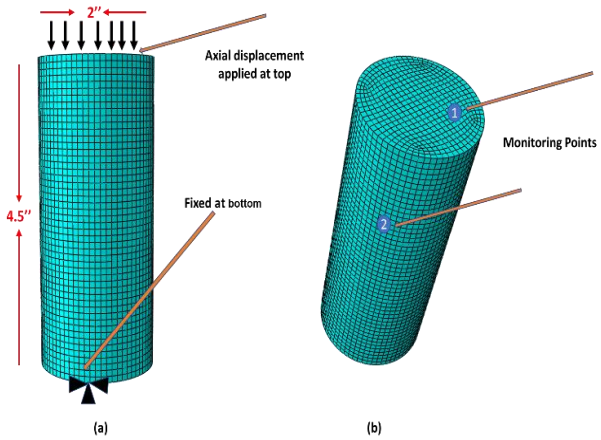

Figure 5. Sketch showing the (a) FEM mesh with geometry dimensions and (b) Monitoring points in the geometry.

3.3 Results of numerical simulation against the experimental data

With the help of the above-mentioned soil models and the corresponding back-calculated constitutive parameters of the frozen sandy clay soil, we were able to perform a numerical analysis of the time-dependent deformation behaviors of frozen soil under the uniaxial compression loading.

Contours of Mises equivalent stress distribution in the samples are given in Figure 6, which shows the stress dependency of two selective strain rates at a constant temperature of -15ºC. Although at this stage, numerical analysis contours are not able to show the brittle cracks formation and ductile deformation, the increase in equivalent stress intensity can be visualized from these contours at different loading rates.

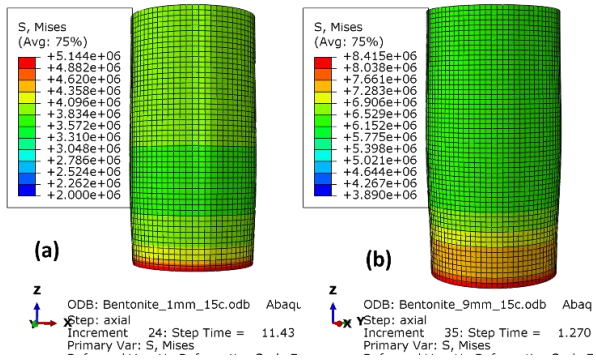

Figure 6. Modeled Mises stress (in Pa) distributions in frozen sandy clayey soil at constant temperature (T= -15ºC) using deformation rates of (a) 1mm/min, and (b) 9mm/min.

Figure 7(a), (b), and (c) shows the relationship between axial stress and axial strain at various constant frozen temperatures under different loading rates. It can be seen from these relationships that the peak strength of frozen soil increases with the decrease of temperature. It is because, with the decrease in temperature, the pore-ice strength increases by making the cementation effects of pore-ice around the solid particles stronger which leads to an increase in the cohesive strength of frozen soil (Kadivar and Manahiloh, 2019). At a constant frozen temperature, the deformation changes from ductile behavior into brittle behavior with the increase of loading rate. Figure 7(a)-(b) shows the post-peak shear softening vanishes with a decrease in temperature, while Figure 7(c) illustrates the phenomenal curve without a post-peak softening deformation mode. Because under the lower loading rate, deformation does not concentrate in the local area but uniformly distributes all over the soil sample. Figure 7 also validate that measured stress-strain relations are properly modeled using linear Drucker-Prager plastic model with Singh-Mitchell creep model, and all three deformation stages (i.e. linear elastic, hardening, and softening behaviors) were captured.

The radial strain is the key parameter controlling the internal dilation and bulking in a frozen soil, which is controlled by the post-peak softening in stress vs. strain relationship. Figure 8(a) and (b) demonstrates the relationship between axial strain versus radial strain at various constant temperatures under different loading rates for both experimental data and simulation results. These plots show that radial strain increases with the decreases of loading rate; however, this phenomenon is more dominant at lower frozen temperatures. The simulation results obtained from the numerical analysis is quite promising with the experimental data before the post-peak strength. Once the peak of strength is achieved, the simulated radial strain versus axial strain plots (Figure 8) falls apart from the experimental data. The reason is because of major cracks and fractures occurrence on the surface of the soil sample during lab testing which cannot be captured in the numerical analysis at this stage. Also, it depends on the position of strain gauges on the soil sample. In numerical analysis, we simply selected the area where the maximum radial strain was produced.

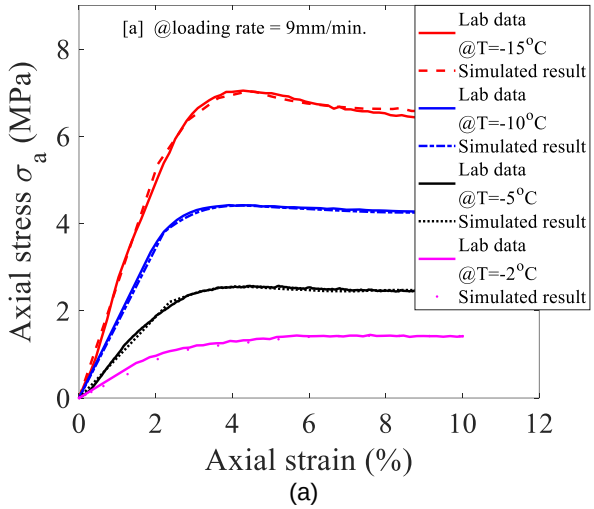

(a)

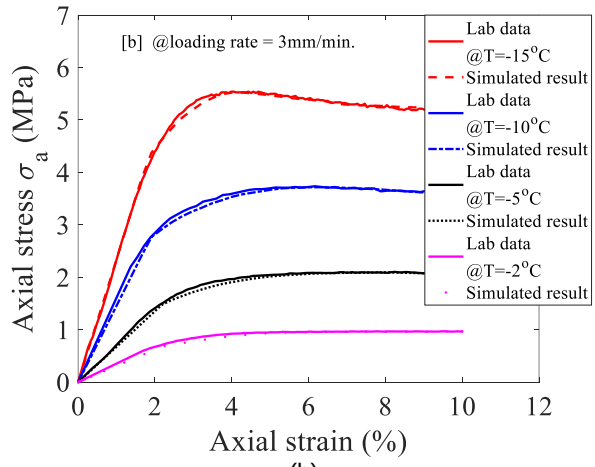

(b)

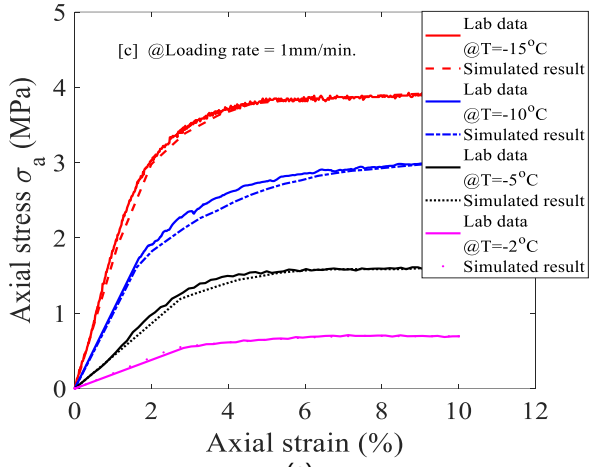

(c)

Figure 7. Relation for measured and modeled stress-strain at various temperatures and loading rates: (a) Loading rate = 9mm/min., (b) Loading rate = 3mm/min., and (c) Loading rate = 1mm/min.

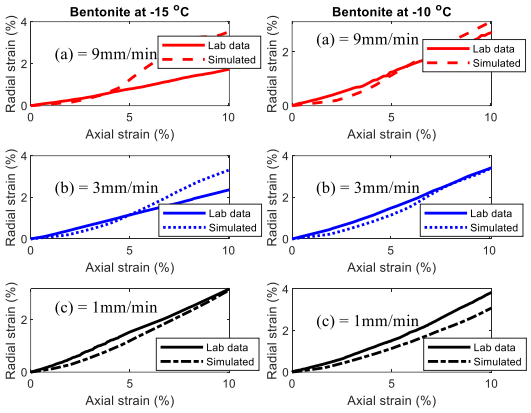

(a)

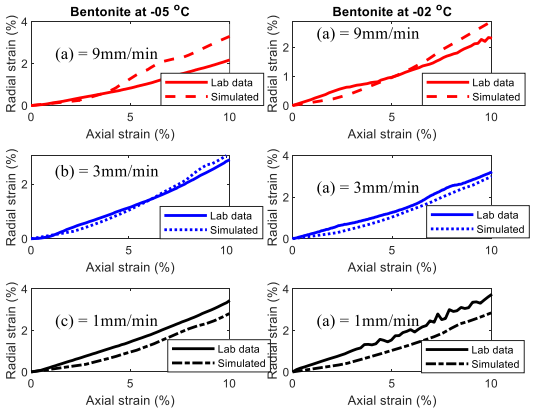

(b)

Figure 8. Relation for measured and modeled axial strain and radial strain curves at various strain rates and temperatures: (a) T = -15ºC and -10ºC, (b) T = -5ºC and -2ºC.

4 CONCLUSIONS

A numerical analysis of the uniaxial compression tests on an artificially frozen clay soil yields promising agreement with measured results. Our results show the effectiveness of using the linear Drucker-Prager model incorporated with the Singh-Mitchell creep model to characterize the strain-rate dependent uniaxial compressive behavior. Our results conclude that low temperatures and a high deformation rate tend to generate brittle failure with post-peak softening behavior. By contrast, a temperature close to the frozen fringe and a low deformation rate results in a diffuse failure associated with strain hardening. The viscous behavior of pore-ice is temperature and loading rate-dependent and dictates the yield strength. The different stress-strain behavior is due to the difference in creep deformation. Our numerical analysis does not include pressure-induced melt behavior, and it is recommended to be included in the future study.

5 ACKNOWLEDGMENTS

The authors would like to acknowledge the supports by Natural Sciences and Engineering Research Council (NSERC) Discovery Grant Canada (NO. RGPIN-2017-05169).

6 REFERENCES

Abaqus. (2016). *Abaqus theory manual*, Version 6.14. Simulia.

Arenson, L.U., Springman, S.M. 2005. Mathematical descriptions for the behavior of ice rich frozen soils at temperatures close to 0 °C. *Candian Geotechnical Journal*, 42 (2), 431–442.

Bolton, M. D. (1986). The Strength and Dilatancy of Sands. *Geotechnique,* 36(1):65–78.

Chen, Y., Azzam, R., Wang, M., Xu, S., and Chang, L. 2011. The uniaxial compressive and tensile tests of frozen saturated clay in Shanghai area. *Environmental Earth Sciences*, 64(1): 29-36. doi: 10.1007/s12665-010-0813-y.

Fei, W., and Yang, Z.J. 2019. Modeling unconfined compression behavior of frozen Fairbanks silt considering effects of temperature, strain rate and dry density. *Cold Regions Science and Technology* ,158: 252-263. doi: https://doi.org/10.1016/j.coldregions.2018.09.002.

Girgis, N. 2019. Experimental investigations on temperature-dependent mechanical properties of artificially frozen sandy clay soils. *MASc thesis*, department of Building, Civil, and Environmental Engineering, Concordia University, Montreal, QC.

Helwany, S. 2007. *Applied soil mechanics with ABAQUS Applications*, John Wiley & Sons.

Hou, F., Lai, Y., Liu, E., Luo, H., and Liu, X. 2018. A creep constitutive model for frozen soils with different contents of coarse grains. *Cold Regions Science and*

Technology, 145: 119-126. doi: https://doi.org/10.1016/j.coldregions.2017.10.013.

Kadivar, M. and Manahiloh, K.N. (2019). Revisiting parameters that dictate the mechanical behavior of frozen soils. *Cold Regions Science and Technology,* 145: 119–126.

Ladanyi, B. 1972. An engineering theory of creep of frozen soils. *Canadian Geotechnical Journal,* 9(1): 63-80. doi: 10.1139/t72-005.

Ladanyi, B., and Benyamina, M.B. 1995. Triaxial relaxation testing of a frozen sand. *Canadian Geotechnical Journal,* 32(3): 496-511. doi: 10.1139/t95-052.

Li, H., Zhu, Y., Zhang, J., and Lin, C. 2004. Effects of temperature, strain rate and dry density on compressive strength of saturated frozen clay. *Cold Regions Science and Technology,* 39(1): 39-45. doi: https://doi.org/10.1016/j.coldregions.2004.01.001.

Li, B. and Wong, R.C.K. 2016. Quantifying Structural States of Soft Mudrocks. *Journal of Geophysical Research: Solid Earth,* 121(5):3324–47. doi:10.1002/ 2015JB012454.

Nixon, J. F. (1991). Discrete Ice Lens Theory for Frost Heave in Soils. *Canadian Geotechnical Journal,* 28(6):843–59.

Wang, S., Qi, J., and Yao, X. 2011. Stress relaxation characteristics of warm frozen clay under triaxial conditions. *Cold Regions Science and Technology,* 69(1): 112-117. doi: https://doi.org/10.1016/j.coldregions.2011.06.015.

Zhu, Y., and Carbee, D.L. 1984. Uniaxial compressive strength of frozen silt under constant deformation rates. *Cold Regions Science and Technology*, 9(1): 3-15.

Zhao, X.D., Zhou, G.Q., Cai, W. and Li, X.J., 2009. Effects of temperature gradients on elastic modulus and compression strength of the saturated frozen clay.*Procedia Earth and Planetary Science,* 1: 420–424.